Absolute fragmentation cross sections in atom-molecule collisions

Chen, T.; Gatchell, M.; Stockett, M. H.; Alexander, J. D.; Zhang, Y.; Rousseau, P.; Domaracka, A.; Maclot, S.; Delaunay, R.; Adoui, L.

Published in:
The Journal of Chemical Physics

DOI:
10.1063/1.4881603

Publication date:
2014

Absolute fragmentation cross sections in atom-molecule collisions: Scaling laws for non-statistical fragmentation of polycyclic aromatic hydrocarbon molecules

T. Chen, M. Gatchell, M. H. Stockett, J. D. Alexander, Y. Zhang, P. Rousseau, A. Domaracka, S. Maclot, R. Delaunay, L. Adoui, B. A. Huber, T. Schlathölter, H. T. Schmidt, H. Cederquist, and H. Zettergren

Citation: The Journal of Chemical Physics **140**, 224306 (2014); doi: 10.1063/1.4881603
View online: http://dx.doi.org/10.1063/1.4881603
View Table of Contents: http://scitation.aip.org/content/aip/journal/jcp/140/22?ver=pdfcov
Published by the AIP Publishing

Absolute fragmentation cross sections in atom-molecule collisions: Scaling laws for non-statistical fragmentation of polycyclic aromatic hydrocarbon molecules

T. Chen,[1] M. Gatchell,[1] M. H. Stockett,[1] J. D. Alexander,[1] Y. Zhang,[2] P. Rousseau,[3,4] A. Domaracka,[3] S. Maclot,[3,4] R. Delaunay,[3,4] L. Adoui,[3,4] B. A. Huber,[3] T. Schlathölter,[5] H. T. Schmidt,[1] H. Cederquist,[1] and H. Zettergren[1,a)]

[1]*Department of Physics, Stockholm University, S-106 91 Stockholm, Sweden*
[2]*Department of Mathematics, Faculty of Physics, M. V. Lomonosov Moscow State University, Leninskie Gory, 119991 Moscow, Russia*
[3]*CIMAP, UMR 6252, CEA/CNRS/ENSICAEN/Université de Caen Basse-Normandie, bd Henri Becquerel, BP 5133, F-14070 Caen Cedex 05, France*
[4]*Université de Caen Basse-Normandie, Esplanade de la Paix, F-14032 Caen, France*
[5]*Zernike Institute for Advanced Materials, University of Groningen, Nijenborgh 4, 9747AG Groningen, The Netherlands*

(Received 5 March 2014; accepted 23 May 2014; published online 9 June 2014)

We present scaling laws for absolute cross sections for non-statistical fragmentation in collisions between Polycyclic Aromatic Hydrocarbons (PAH/PAH$^+$) and hydrogen or helium atoms with kinetic energies ranging from 50 eV to 10 keV. Further, we calculate the total fragmentation cross sections (including statistical fragmentation) for 110 eV PAH/PAH$^+$ + He collisions, and show that they compare well with experimental results. We demonstrate that non-statistical fragmentation becomes dominant for large PAHs and that it yields highly reactive fragments forming strong covalent bonds with atoms (H and N) and molecules (C_6H_5). Thus nonstatistical fragmentation may be an effective initial step in the formation of, e.g., Polycyclic Aromatic Nitrogen Heterocycles (PANHs). This relates to recent discussions on the evolution of PAHNs in space and the reactivities of defect graphene structures. © *2014 AIP Publishing LLC*. [http://dx.doi.org/10.1063/1.4881603]

I. INTRODUCTION

When complex molecules are heated through interactions with energetic atoms/ions, photons, or electrons, the excess energy is typically redistributed over all internal degrees of freedom before the decay. This is often referred to as statistical decay.[1] *Non-statistical* decay processes may on the other hand be induced in low energy collisions with heavy particles such as atoms, molecules, or their ions. Direct evidence for this was first observed in C_{60}^- + He/Ne[2,3] and more recently in C_{60}^+ + Ne and PAH$^+$ + He collisions.[4,5] The picture here is that single atoms are knocked out in binary nuclear interactions during the femtosecond timescales of the collisions.

For fullerenes (C_{60}) and Polycyclic Aromatic Hydrocarbons (PAHs) (see Fig. 1), the dissociation energies for single carbon (or CH_x) knockout are much higher than for the lowest energy dissociation channels favoured in statistical decay processes.[4] Observations of one carbon atom losses are thus clear signatures of non-statistical fragmentation. Micelotta *et al.* have proposed[6] that PAHs may be processed in this way when exposed to ionized hydrogen and helium in plasma shocks from supernova explosions. Partly damaged large PAHs may then, e.g., serve as a possible pathway for the formation of nitrogen-substituted PAHs—so called PANHs (Polycyclic Aromatic Nitrogen Heterocycles).

Recently, Postma *et al.* carried out molecular dynamics simulations of interactions between H or He and anthracene ($C_{14}H_{10}$) at astrophysically relevant collision energies.[7] They found that the threshold for carbon knockouts is significantly higher (about 27 eV) than what was assumed by Micelotta *et al.* (7.5 eV),[6] and that below threshold nuclear stopping processes may induce significant statistical fragmentation. Based on the results from a statistical model where fragmentation and IR-emission processes compete, Postma *et al.* concluded that knockouts only give minor contributions to the total fragmentation cross sections for small PAHs like anthracene $C_{14}H_{10}$.[7] Further, as substantial fractions of these fragments are expected to decay further it was concluded that PANH formation from small PAHs is highly unlikely.[7] Here, we will argue that this is not the case for *large* PAHs where the probability for survival of fragments from single carbon knockout is higher, and where PANH-formation thus could be important.

Statistical fragmentation is expected to become less important for large PAHs due to their large heat capacities. The absolute cross section for non-statistical processes, however, increases linearly with the number of atoms in the molecule. This has recently been demonstrated in 110 eV PAH$^+$ + He collisions,[5] where a large fraction of the observed fragments are due to non-statistical processes. In the present work, we have studied these intriguing issues by calculating electronic and nuclear energy losses due to collisions between H or He and nine PAHs, benzene or naphthalene (see Fig. 1) in the

a)Author to whom correspondence should be addressed. Electronic mail: henning@fysik.su.se

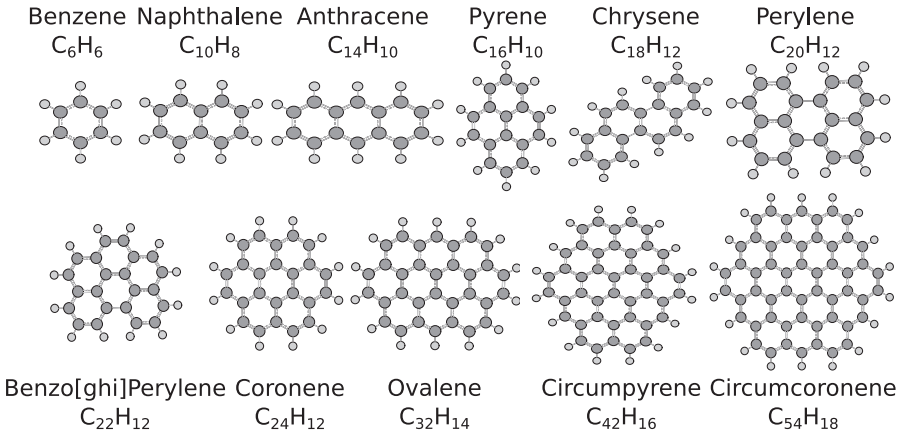

FIG. 1. Benzene, naphthalene, and nine planar polycyclic aromatic hydrocarbons (PAHs) are considered in this work (see text).

energy range between 50 eV and 10 keV. We use these results to establish simple scaling laws for the absolute cross sections for non-statistical fragmentation in PAH/PAH$^+$ + H and PAH/PAH$^+$ + He collisions. Further, we present results on the different reactivities of intact ($C_{54}H_{18}$) and defect ($C_{53}H_{18}$) circumcoronene with N, H, and C_6H_5 using Density Functional Theory (DFT).

II. THEORY

A. Molecular structure calculations

Molecular structure calculations have been carried out using DFT, as implemented in the Gaussian 09 package.[8] The B3LYP functional[9,10] was used to calculate the molecular properties of intact PAHs. This functional is known to accurately describe the electronic properties of carbon clusters,[11] fullerenes,[12–14] and PAHs.[15–17] Molecular geometries were optimized using the 6-311++G(2*d*,*p*)[8] basis set, followed by frequency calculations. The coordinates of the nuclei were used in the nuclear stopping calculations, and the molecular orbital coefficients were used to calculate the valence electron densities for the electronic stopping calculations. In the latter case, we used a smaller basis set (6-31G*),[8] which significantly reduces the computational cost while introducing only minor deviations from the results with the larger basis set.

The M06-L functional[18] was used to calculate the molecular structures of circumcoronene after prompt removal of an inner carbon atom and the reactivity of such a defect PAH structure following its relaxation to a minimum on the potential energy surface. This functional was recently used in related studies of defect graphene structures,[19] which allows for a direct comparison with the present results. The fragment geometries were optimized using the 6-31G* basis set, followed by frequency calculations in order to verify that they correspond to minima on the potential energy surfaces (all real frequencies) and to take the zero-point vibrational energies into account.

B. Nuclear stopping

The present collision model is evaluated by means of Monte Carlo simulations. Collision geometries are generated randomly to ensure that all orientations of the molecule are equally likely just as in the experiments.[20] The model treats collisions between *neutral* PAHs and atoms, while the PAHs are singly charged in the experiments. However, due to the large number of delocalized π-electrons the charge is expected to play a minor role in the stopping processes. Indeed, we will show that the model and experimental results are in good agreement, which suggest that the model results may be used for both neutral and singly charged systems.

The interactions between the colliding atom and the nuclei of the individual atoms in the PAH molecule are described by screened Coulomb potentials,

$$V(r) = \frac{Z_1 Z_2}{r} f(x), \tag{1}$$

where Z_1 (projectile) and Z_2 (target) are the atomic numbers of the collision partners, r is the distance between the projectile and the target, and $f(x)$ is a screening function. In the present work we use the ZBL (Ziegler, Biersack, Littmark)[21] and the Lindhard[22] screening functions. The ZBL is most commonly used to describe ion-solid interactions.[21] With the Lindhard screening function it is possible to derive an analytical relation between the impact parameter p (with respect to an atom in the molecule) and the energy transfer to this atom. This result is then used to establish scaling formulas for non-statistical fragmentation of PAHs. The ZBL screening function is

$$f_{ZBL}(x) = 0.1818e^{-3.2x} + 0.5099e^{-0.9423x} + 0.2802e^{-0.4029x} + 0.02817e^{-0.2016x}, \tag{2}$$

where

$$x = \frac{r}{a_{ZBL}} = \frac{r\left(Z_1^{0.23} + Z_2^{0.23}\right)}{0.8853 a_0} \tag{3}$$

and a_{ZBL} is the so called screening length.

The Lindhard screening function is

$$f_{Lindhard}(x) = \frac{k_s}{s} x^{1-s}, \tag{4}$$

where k_s is a constant which depends on the integer value s,[22] and

$$x = \frac{r}{a_{Lindhard}} = \frac{r\sqrt{Z_1^{2/3} + Z_2^{2/3}}}{0.8853 a_0}. \quad (5)$$

Here, the screening length is denoted $a_{Lindhard}$ (a_0 is the Bohr radius).

We now consider an elastic collision in which an atom with atomic number Z_1, mass M_1, and kinetic energy E in the laboratory system collides with an atom with atomic number Z_2, and mass M_2 at rest. The (nuclear) energy transfer to M_2 is

$$T_{nuc} = T_{max} \sin^2 \frac{\phi}{2}, \quad (6)$$

where ϕ is the scattering angle in the center-of-mass system and T_{max}, the maximum energy transfer (head-on collision), is

$$T_{max} = \frac{4 M_1 M_2}{(M_1 + M_2)^2} E. \quad (7)$$

The scattering angle ϕ and the impact parameter, p, are related through

$$\sin \frac{\phi}{2} = \cos \left(\int_{r_{min}}^{\infty} \frac{p dr}{r^2 \sqrt{1 - \frac{V(r)}{E_{CM}} - (\frac{p}{r})^2}} \right), \quad (8)$$

where

$$E_{CM} = \frac{M_2}{M_1 + M_2} E \quad (9)$$

is the initial kinetic energy in the Center-of-Mass (CM) system, and r_{min} is the distance of closest approach. The latter is given by

$$1 - \frac{V(r_{min})}{E_{CM}} - \left(\frac{p}{r_{min}} \right)^2 = 0. \quad (10)$$

There is no closed expression for ϕ with the ZBL potential (Eq. (2)). For the Lindhard potential (cf. Eq. (4)), however, we give an analytical expression which connects the scattering angle ϕ and the impact parameter p. We set $s = 2$ and $k_s = k_2 = 0.831$,[2] and obtain

$$\sin \frac{\phi}{2} = \cos \frac{\pi p}{2\sqrt{p^2 + p_0^2}}, \quad (11)$$

where

$$p_0^2 = \frac{0.831 a_{Lindhard} Z_1 Z_2}{2 E_{CM}}. \quad (12)$$

Equations (6) and (11) give the geometrical cross section for energy transfer above a threshold energy E_{th},

$$\sigma = \pi p^2 = \frac{4\pi p_0^2}{\pi^2 \arccos^{-2}(\sqrt{E_{th}/T_{max}}) - 4}. \quad (13)$$

Thus by using the threshold energies for single C- and single H-knockout, Eq. (13) gives the non-statistical fragmentation cross section per C- and H-atom in the molecule without numerical integration of Eq. (8). Here, we use the results from molecular dynamics simulations of $C_{14}H_{10} + He/H$ collisions,[7] and set the threshold energies to 27 eV and 9 eV for C- and H-knockout, respectively.

C. Electronic stopping

We follow Postma *et al.*[23] and calculate the electronic stopping with the aid of well-known formulas for atom-solid interactions. The large number of electrons in the PAHs are described as a free electron gas, which is characterized by the so-called one-electron radius,

$$r_s = \left(\frac{3}{4\pi n_0} \right)^{\frac{1}{3}}. \quad (14)$$

Here n_0 is the valence electron density, which we obtain from molecular structure calculations using DFT (cf. Sec. II A). For the present collision energies, we assume that the energy loss due to inelastic interactions with the electrons, T_e, is proportional to the projectile velocity, v.[24] The electronic stopping power is then

$$\frac{dT_e}{dR} = \gamma(r_s) v, \quad (15)$$

where $\gamma(r_s)$ is the friction coefficient which is related to the scattering phase shifts (δ_l) through

$$\gamma(r_s) = \frac{3}{k_F r_s^3} \sum_{l=0}^{\infty} (l+1) \sin^2(\delta_l - \delta_{l+1}) \quad (16)$$

and k_F is the length of the Fermi wave vector.[25] Puska and Nieminen[25] have calculated the friction coefficients for atoms embedded in a homogeneous electron gas for a few different r_s-values (different electron densities). Here, we use a fit to their results to calculate the stopping power for any electron density. Thus for each point along the random trajectories through the PAH molecular electron clouds, we calculate the electronic stopping power from Eq. (15) and multiply by the step-size to get the stopping energy. At the same time, we calculate the nuclear stopping energy (cf. Sec. II B) and the total stopping energy is taken as the sum of these two contributions for each individual trajectory.

III. RESULTS AND DISCUSSION

A. Comparisons with experimental results

In Fig. 2 we show the mass spectra for 11 keV $He^+ + C_{24}H_{12}$ collisions (upper panel) and for $C_{24}H_{12}^+ + He$ collisions at a center-of-mass energy of 110 eV (lower panel). The higher energy spectrum was recorded at the ARIBE facility (GANIL), in Caen (France). Briefly, the He^+-ions are produced with an ECR ion source and collide with a neutral target of $C_{24}H_{12}$-molecules. The charged collision products are then analyzed with the aid of a linear time-of-flight spectrometer (for details see Refs. 26 and 27 and references therein). The 110 eV spectrum was recorded at Stockholm University (Sweden) using an electrospray ionization source to produce PAH cation beams (see Refs. 4 and 5 for details). The PAH^+ ions are mass selected and guided to a collision cell containing He gas. The intensities of intact PAH^+ ions and charged fragments are then measured behind the gas cell by means of two sets of horizontal deflector plates, adjustable slits, and a position sensitive detector. The absolute PAH^+ fragmentation cross sections are measured by monitoring the loss of

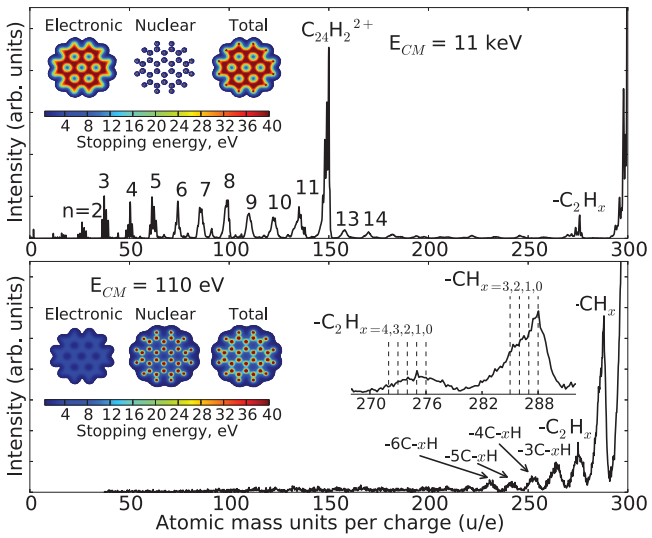

FIG. 2. Upper: Mass to charge spectrum for $He^+ + C_{24}H_{12}$ collisions at 11 keV center-of-mass energy. The $C_nH_x^+$ fragments are labeled by the number of carbon atoms (n). Lower: Mass to charge spectrum for $C_{24}H_{12}^+$+He collisions at 110 eV center-of-mass energy. The insets show results from the present stopping calculations (see text) and a zoom-in of the large fragment mass distribution (lower panel). The peak widths in the lower panel partly reflect the fragment kinetic energy distributions and partly the contributions from fragments with different number of H-atoms.

ion beam intensities as functions of the pressure in the collision cell (beam attenuation method[4,5]). This was done with narrow slits such that the pure hydrogen-loss channels were included in the attenuation cross sections and with broad slits to get the separate absolute cross section for carbon loss. The latter method was used to obtain the single carbon loss cross sections. These are presented for the first time here while the total cross sections have been reported earlier.[5]

The insets in Fig. 2 show the results from the present stopping calculations for face-on atom trajectories through the coronene molecule. In the high energy case (upper panel), electronic stopping extends to above 40 eV and dominates the energy transfer to the molecule. The electronic excitation is induced locally along the ion trajectories on the sub femtosecond timescales and is rapidly redistributed across all internal degrees of freedom. As the internal energy is typically 40 eV, i.e., well above the lowest dissociation energy channels at about 5 eV[17] (loss of H or C_2H_2) a large fraction of the collisions will lead to statistical fragmentation processes in the 11 keV case. This readily explains the rich distribution of fragments in the mass spectrum in the upper panel of Fig. 2.

The fragment mass spectrum is markedly different in the lower panel of Fig. 2. Here, the fragment distribution is shifted towards higher masses, suggesting that the coronene molecules on the average now are much colder. Here, typical electronic stopping energies are only about 4 eV and it is unlikely that they alone could lead to fragmentation on microsecond timescales. However, they do add to the nuclear stopping energies and as they are substantially larger than the PAH cation HOMO-LUMO gap (e.g., 1.1 eV for $C_{24}H_{12}^+$) we will take electronic stopping into account in the following discussions. The most prominent fragment peak in the 110 eV case (lower panel) is due to the loss of a single heavy atom ($-CH_x$, $x = 0,1,\ldots$). This is a clear signature of non-statistical fragmentation in which a single carbon atom or a CH-group is knocked out,[4,5] possibly followed by statistical loss of one or a few H-atoms.

According to the molecular dynamics simulations by Postma *et al.*,[7] only nuclear stopping above about 27 eV will lead to prompt non-statistical carbon knockout. Indeed a substantial fraction of the trajectories exceed this threshold at 110 eV according to the present calculations. By taking the ratio between the number of such trajectories and the total number of trajectories times the area through which the latter are launched, we arrive at an absolute model cross section for single carbon knockout.

The single carbon knockout cross sections as functions of the number of carbon atoms in the PAH molecules are shown in the left part of Fig. 3. The ZBL and Lindhard screening functions give similar results and are close to the experimental cross sections for single carbon knockout by He. The model results are within the error bars of the cross section for the largest PAHs, but somewhat higher than the experimental cross sections for the smaller PAHs (left panel of Fig. 3).

In the right panel of Fig. 3, we show calculated cross sections for single hydrogen knockouts (9 eV threshold). In this case the results using the screened Bohr potential are slightly higher than those for the ZBL potential. As single H-loss also is a strong statistical fragmentation channel, it is not possible to unambiguously determine separate H-atom knockout cross sections from the experiment.

The total ZBL model knockout cross sections are the sums of the corresponding results in the left and right panels of Fig. 3 and are shown as open squares in Fig. 4. We model the *total* fragmentation cross section (including also statistical processes) relying on results from direct measurements of the internal energies of anthracene ($C_{14}H_{10}$) fragmentation.[28] It was then established that 10 eV internal excitation energy was needed for statistical fragmentation on the microsecond time scale.[28] Here, we assume an Arrhenius type decay and

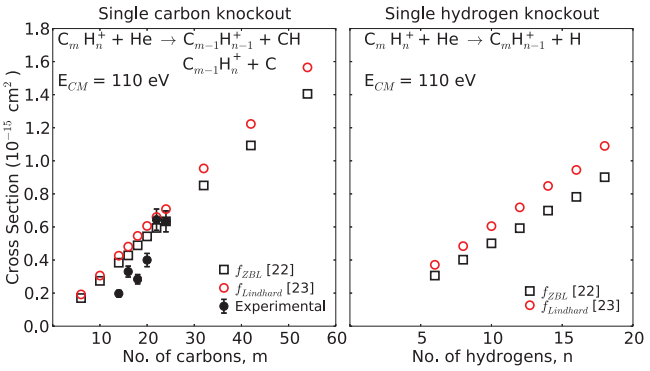

FIG. 3. Absolute single carbon and single hydrogen knockout cross sections as functions of the number of carbon (left) and hydrogen (right) atoms in the PAH molecule. The former has contributions from knockouts of inner (C) and outer (CH) carbon atoms. The open squares and circles are model results using the ZBL and Lindhard screening functions for binary nuclear interactions in PAH/PAH^+ + He collisions at a center-of-mass energy of 110 eV (see text). The experimental cross sections for single carbon knockout are shown as solid circles.

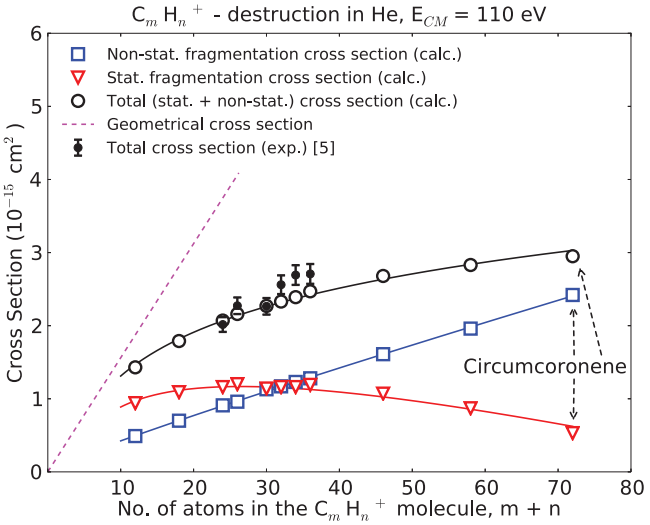

FIG. 4. The total model (open circle) and experimental[5] (solid circles) fragmentation cross sections for PAH/PAH$^+$ + He collisions at a center-of-mass energy of 110 eV. The geometrical cross sections were estimated by enclosing coronene in an infinitely thin circular disk, assumed to be randomly oriented in the collision,[20] and by linear scaling with PAH size. The separate contributions from statistical (open triangles) and non-statistical (open squares) fragmentation processes refer to the model results (see text).

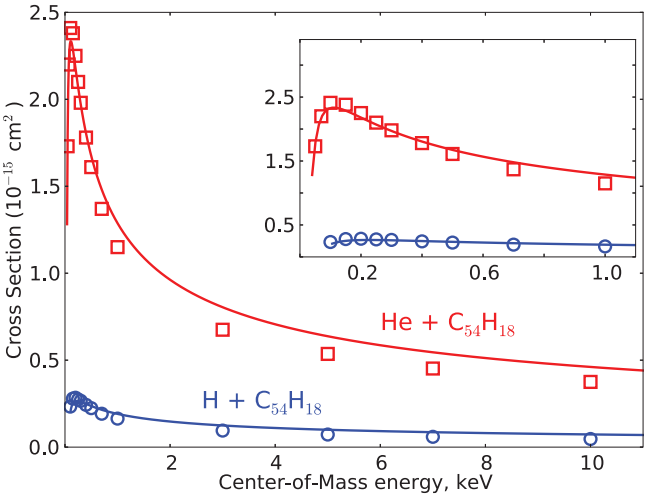

FIG. 5. The non-statistical atom knockout cross sections as functions of center-of-mass energy for H+$C_{54}H_{18}$ and He + $C_{54}H_{18}$ collisions. The open symbols are from Monte-Carlo simulations using the ZBL potential. The solid lines are the present scaling laws (Eqs. (17) and (18)).

scale this result with the number of degrees of freedom. The statistical threshold energy is then $T_{th}^{stat}(N) = [(3N-6)/(3\times 24-6)]\times 10$ eV, where $N = m + n$ is the number of atoms in the C_mH_n molecule. This approach relies on the assumption that the lowest dissociation energies (H- and C_2H_2-loss) are similar for different PAHs, which indeed seems to be the case.[17]

In the present simulations, a statistical fragmentation event is assumed to result from a trajectory where the total stopping is larger than the statistical threshold energy (T_{th}^{stat}), but where the energy losses to the individual nuclei (T_{nuc}) all are smaller than the threshold energy for prompt atom knockout. The resulting model and the experimental total destruction cross sections in Fig. 4 are in excellent agreement, and in this intermediate PAH size region (N=25–35) about 50% of the total destruction cross section is due to single atom knockouts. For large PAHs, like circumcoronene $C_{54}H_{18}$ with $N = 72$ and beyond, the total destruction cross section is dominated by non-statistical fragmentation. This is because the statistical threshold energy increases as a function of PAH size, while the knockout thresholds are size independent. Note that the total destruction cross sections are significantly smaller than estimates of the geometrical cross sections at 110 eV (dashed line in Fig. 4). That is the PAHs are partially transparent to He-atoms in this collision energy range. This is consistent with the inset shown in the lower panel of Fig. 2, where electronic stopping energies typically are below 4 eV for 110 eV collisions. Only trajectories close to the individual nuclei will then lead to fragmentation on the experimental time scale.

B. Scaling laws for non-statistical PAH fragmentation

The present scaling laws are based on fits to the results from simulations of He+$C_{54}H_{18}$ and H+$C_{54}H_{18}$ collisions using the ZBL potential at different center-of-mass energies (cf. Fig. 5). The scaling laws are

$$\sigma_{non\text{-}stat}^{H+PAH} = 0.44 \times \left(m\sigma_m^{H+C} + n\sigma_n^{H+H}\right) \quad (17)$$

and

$$\sigma_{non\text{-}stat}^{He+PAH} = 0.74 \times \left(m\sigma_m^{He+C} + n\sigma_n^{He+H}\right), \quad (18)$$

for arbitrary C_mH_n-molecules colliding with H and He, respectively. Here, σ_m and σ_n are the cross sections for transferring energies above E_{th} (=27 eV) to a C atom and above E_{th} (=9 eV) to a H atom according to Eq. (13),

$$\sigma = \pi p^2 = \frac{4\pi p_0^2}{\pi^2 \arccos^{-2}(\sqrt{E_{th}/T_{max}}) - 4}.$$

This analytical expression was derived with the Lindhard screening function while the scaling laws are fits to Monte Carlo results using the ZBL screening function. The close agreement between the Lindhard and ZBL results shown in Fig. 3 motivates this approach. The ZBL results were used for the fits in Fig. 5 as this screeening function in general gives better results for interactions with solids. The inset in Fig. 5 shows that the scaling law performs particularly well in the 50 eV to 1 keV center of mass energy range.

The performance of the scaling laws is further illustrated in Fig. 6, where the left and right panels show comparisons of the Monte Carlo simulation results with those from the scaling laws for PAH/PAH$^+$+H and PAH/PAH$^+$+He collisions at center-of-mass energies of 100 eV and 1 keV, respectively. The maximum error is less than 20% in the 50 eV to 1 keV range, i.e., on the order of typical systematic errors in related experiments.[4,5] This shows that the scaling laws give good results for a wide range of PAH sizes.

C. Reactivities of defect PAHs

The experimental results clearly show that large PAHs may survive on long timescales after prompt atom knockouts. Although the lifetimes have not yet been measured, it

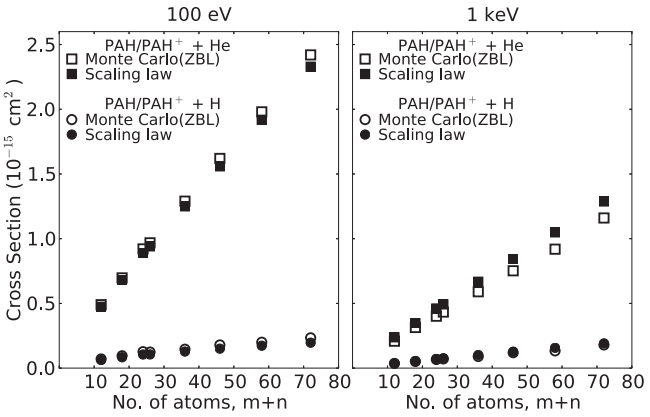

FIG. 6. The non-statistical absolute fragmentation cross sections as functions of PAH size for PAH/PAH$^+$+H and PAH/PAH$^+$+He collisions at center-of-mass energies of 100 eV (left panel) and 1 keV (right panel). The open and solid symbols are from the Monte Carlo simulations and from the present scaling laws (Eqs. (17) and (18)), respectively.

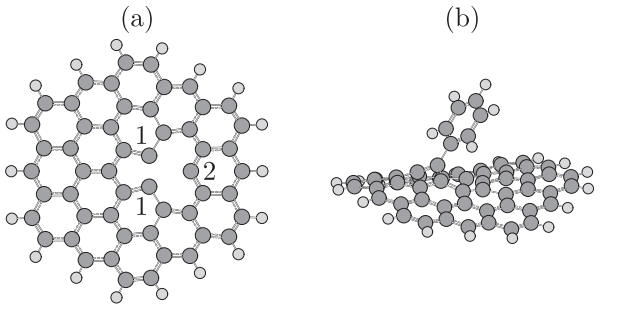

	$C_{54}H_{18}/C_{54}H_{18}^+ + X$ Pos 1	Pos 2	$C_{53}H_{18}/C_{53}H_{18}^+ + X$ Pos 1	Pos 2
X = H	0.35/1.10	0.32/0.95	4.14/4.39	4.04/4.19
X = N	1.78/1.25	1.60/1.81	12.11/13.40	
X = C_6H_5	0.21/0.88	0.19/0.70	4.03/4.39	3.81/4.08

FIG. 7. (a) Optimized circumcoronene structure after removal of a single carbon atom ($C_{53}H_{18}$). The defect PAH-molecule has two different reactive sites labelled 1 and 2. (b) Molecular structure after attachment of a C_6H_5 molecule to the most reactive site (position 1). The table shows the binding energies (in eV) of H- and N-atoms, and C_6H_5-molecules to $C_{54}H_{18}$, $C_{54}H_{18}^+$, $C_{53}H_{18}$, and $C_{53}H_{18}^+$. The nitrogen atom is bound to three carbon atoms in $C_{53}H_{18}$ and $C_{53}H_{18}^+$, yielding planar PANH molecules.

has been demonstrated that, e.g., $C_{23}H_{12}^+$ survives on the experimental microsecond timescales (cf. Fig. 2). Larger systems are expected to survive on even longer (>ms) timescales such that radiative cooling becomes competitive.[29] In addition, the most prominent fragmentation pathway for large pericondensed PAHs (e.g., circumcoronene) is through emission of H-atoms and/or H_2-molecules. This means that defects due to removal of inner carbons in PAHs are expected to survive until the PAHs are further damaged due to secondary radiation processes or react with atoms/molecules to form larger molecules.

We have therefore investigated the reactivities of intact ($C_{54}H_{18}$ and $C_{54}H_{18}^+$) and defect ($C_{53}H_{18}$ and $C_{53}H_{18}^+$) circumcoronene with N- and H- atoms and with C_6H_5-molecules using DFT (see Sec. II A). In Fig. 7(a) we show the relaxed $C_{53}H_{18}$ structure after prompt inner carbon knockout. This gives three carbon atoms with dangling bonds corresponding to two different reactive sites (position 1 and position 2). We have added single H- and N-atoms, or C_6H_5-molecules to these sites and we then let these systems relax, as the example in Fig. 7(b) illustrates. We find that the binding energies are slightly higher for position 1 than for position 2, and up to a factor of ten higher than for intact circumcoronene (see the lower part of Fig. 7). The singly charged systems display similar trends as the neutral systems. The binding energies are somewhat higher except for the binding of N to position 1 of intact $C_{54}H_{18}^+$, which has a slightly lower binding energy compared to the corresponding neutral system.

Our results are consistent with recent theoretical studies of graphene structures, which show that the binding energies of H-atoms to intact and defect graphene is 0.72 eV and 4.29 eV, respectively.[19] The corresponding values for binding of C_6H_5-molecules to graphene are 0.38 eV and 3.82 eV.[19] We find that the binding energy of nitrogen (12.11 eV) to defect circumcoronene is significantly higher than these values. The reason being that nitrogen becomes bound to all three C-atoms in positions 1 and 2 in $C_{53}H_{18}$ (see Fig. 7(a)), forming a planar PANH structure, $C_{53}NH_{18}$. Thus the stabilities and reactivities of large defect PAHs show that knockout processes may serve as an important initial step in the formation of, e.g., PANHs and in the growths of three-dimensional structures (see Fig. 7(b)). The presence of PANHs in the interstellar medium may be important for explaining the observed widths of the so-called Aromatic Infrared Bands (AIBs) along some lines of sight.[30]

IV. SUMMARY AND CONCLUSIONS

In summary, we have calculated the nuclear and electronic energy transfers for PAH/PAH$^+$ + He and PAH/PAH$^+$ + H collisions in the 0.05–10 keV center-of-mass energy range by combining molecular structure calculations with well-established models from ion/atom-solid interactions. We show that nuclear stopping dominates at low collision energies (<1 keV) and that a substantial fraction of the total PAH destruction cross section is due to non-statistical atom knockout processes, in agreement with experimental results. At higher collision energies, electronic stopping dominates, leading to statistical fragmentation of isolated PAHs. However, non-statistical processes are expected to be important even for energies above 1 keV when PAHs are embedded in a surrounding environment (e.g., in clusters). The electronic stopping energy may then be redistributed among the cluster constituents[26,31–35] such that defect PAHs may survive long enough for further reactions.[34,35] Our molecular structure calculations show that these defects act like sponges for atoms and molecules, and may thus serve as important intermediates in the formation of larger molecules from smaller ones. Here, we present simple scaling laws for the non-statistical fragmentation cross sections in PAH/PAH$^+$ + He/H collisions. These expressions may be used to reveal the importance of such processes in vacuum and in various types of environments, for instance in the formation of PANHs

(nitrogen containing PAHs) from large PAHs exposed to plasma shock waves from supernova explosions.[36]

ACKNOWLEDGMENTS

This work was supported by the Swedish Research Council (Contract Nos. 621-2012-3662, 621-2012-3660, and 621-2011-4047). We acknowledge the COST action CM1204 "XUV/X-ray light and fast ions for ultrafast chemistry (XLIC)" and the European Associated Laboratory DYNAMO.

[1] K. Hansen, *Statistical Physics of Nanoparticles in the Gas Phase* (Springer, 2013).
[2] M. C. Larsen, P. Hvelplund, M. O. Larsson, and H. Shen, Eur. Phys. J. D **5**, 283 (1999).
[3] S. Tomita, P. Hvelplund, S. B. Nielsen, and T. Muramoto, Phys. Rev. A **65**, 043201 (2002).
[4] M. Gatchell, M. H. Stockett, P. Rousseau, T. Chen, K. Kulyk, H. T. Schmidt, J. Y. Chesnel, A. Domaracka, A. Mery, S. Maclot, L. Adoui, K. Stochkel, P. Hvelplund, Y. Wang, M. Alcamí, B. A. Huber, F. Martí, H. Zettergren, and H. Cederquist, Int. J. Mass Spectrom. **365–366**, 260 (2014).
[5] M. H. Stockett, H. Zettergren, L. Adoui, J. D. Alexander, U. Berzins, T. Chen, M. Gatchell, N. Haag, B. A. Huber, P. Hvelplund, A. Johansson, H. A. B. Johansson, K. Kulyk, S. Rosen, P. Rousseau, K. Stochkel, H. T. Schmidt, and H. Cederquist, Phys. Rev. A **89**, 032701 (2014).
[6] E. R. Micelotta, A. P. Jones, and A. G. G. M. Tielens, Astronom. Astrophys. **510**, A36 (2010).
[7] J. Postma, R. Hoekstra, A. Tielens, and T. Schlathölter, Astrophys. J. **783**, 61 (2014).
[8] M. J. Frisch, G. W. Trucks, H. B. Schlegel *et al.*, Gaussian 09, Revision A.1, Gaussian Inc., Wallingford, CT, 2009.
[9] A. D. Becke, J. Chem. Phys. **98**, 5648 (1993).
[10] C. Lee, W. Yang, and R. G. Parr, Phys. Rev. B **37**, 785 (1988).
[11] S. Díaz-Tendero, F. Martín, and M. Alcamí, J. Phys. Chem. A **106**, 10782 (2002).
[12] S. Díaz-Tendero, F. Martín, and M. Alcamí, Phys. Rev. Lett. **95**, 013401 (2005).
[13] S. Díaz-Tendero, F. Martín, and M. Alcamí, J. Chem. Phys. **123**, 184306 (2005).
[14] H. Zettergren, G. Sánchez, S. Díaz-Tendero, M. Alcamí, and F. Martín, J. Chem. Phys. **127**, 104308 (2007).
[15] S. R. Langhoff, J. Phys. Chem. **100**, 2819 (1996).
[16] C. W. Bauschlicher, Jr., D. M. Hudgins, and L. J. Allamandola, Theor. Chem. Acc. **103**, 154 (1999).
[17] A. I. S. Holm, H. A. B. Johansson, H. Cederquist, and H. Zettergren, J. Chem. Phys. **134**, 044301 (2011).
[18] Y. Zhao and D. Truhlar, Theor. Chem. Accounts **120**, 215 (2008).
[19] P. A. Denis and F. Iribarne, J. Phys. Chem. C **117**, 19048 (2013).
[20] B. O. Forsberg, J. D. Alexander, T. Chen, A. T. Pettersson, M. Gatchell, H. Cederquist, and H. Zettergren, J. Chem. Phys. **138**, 054306 (2013).
[21] J. F. Ziegler, J. P. Biersack, and U. Littmark, *The Stopping and Range of Ions in Matter* (Pergamon, 1985).
[22] J. Lindhard, V. Nielsen, and M. Scharff, Mat. Fys. Medd. Dan. Vid. Selsk. **36**, 10 (1968).
[23] J. Postma, S. Bari, R. Hoekstra, A. G. G. M. Tielens, and T. Schlathölter, Astrophys. J. **708**, 435 (2010).
[24] T. L. Ferrell and R. H. Ritchie, Phys. Rev. B **16**, 115 (1977).
[25] M. J. Puska and R. M. Nieminen, Phys. Rev. B **27**, 6121 (1983).
[26] A. I. S. Holm, H. Zettergren, H. A. B. Johansson, F. Seitz, S. Rosén, H. T. Schmidt, A. Ławicki, J. Rangama, P. Rousseau, M. Capron, R. Maisonny, L. Adoui, A. Méry, B. Manil, B. A. Huber, and H. Cederquist, Phys. Rev. Lett. **105**, 213401 (2010).
[27] A. Ławicki, A. I. S. Holm, P. Rousseau, M. Capron, R. Maisonny, S. Maclot, F. Seitz, H. A. B. Johansson, S. Rosén, H. T. Schmidt, H. Zettergren, B. Manil, L. Adoui, H. Cederquist, and B. A. Huber, Phys. Rev. A **83**, 022704 (2011).
[28] S. Martin, L. Chen, R. Bredy, G. Montagne, C. Ortega, T. Schlathölter, G. Reitsma, and J. Bernard, Phys. Rev. A **85**, 052715 (2012).
[29] K. Hansen and E. Campbell, J. Chem. Phys. **104**, 5012 (1996).
[30] D. M. Hudgins, C. W. Bauschlicher, and L. J. Allamandola, Astrophys. J. **632**, 316 (2005).
[31] B. Manil, L. Maunoury, B. A. Huber, J. Jensen, H. T. Schmidt, H. Zettergren, H. Cederquist, S. Tomita, and P. Hvelplund, Phys. Rev. Lett. **91**, 215504 (2003).
[32] H. Zettergren, H. T. Schmidt, P. Reinhed, H. Cederquist, J. Jensen, P. Hvelplund, S. Tomita, B. Manil, J. Rangama, and B. A. Huber, Phys. Rev. A **75**, 051201 (2007).
[33] H. A. B. Johansson, H. Zettergren, A. I. S. Holm, F. Seitz, H. T. Schmidt, P. Rousseau, A. Lawicki, M. Capron, A. Domaracka, E. Lattouf, S. Maclot, R. Maisonny, B. Manil, J.-Y. Chesnel, L. Adoui, B. A. Huber, and H. Cederquist, Phys. Rev. A **84**, 043201 (2011).
[34] H. Zettergren, P. Rousseau, Y. Wang, F. Seitz, T. Chen, M. Gatchell, J. D. Alexander, M. H. Stockett, J. Rangama, J. Y. Chesnel, M. Capron, J. C. Poully, A. Domaracka, A. Méry, S. Maclot, H. T. Schmidt, L. Adoui, M. Alcamí, A. G. G. M. Tielens, F. Martín, B. A. Huber, and H. Cederquist, Phys. Rev. Lett. **110**, 185501 (2013).
[35] F. Seitz, H. Zettergren, P. Rousseau, Y. Wang, T. Chen, M. Gatchell, J. D. Alexander, M. H. Stockett, J. Rangama, J. Y. Chesnel, M. Capron, J. C. Poully, A. Domaracka, A. Mery, S. Maclot, V. Vizcaino, H. T. Schmidt, L. Adoui, M. Alcami, A. G. G. M. Tielens, F. Martin, B. A. Huber, and H. Cederquist, J. Chem. Phys. **139**, 034309 (2013).
[36] A. G. G. M. Tielens, Rev. Mod. Phys. **85**, 1021 (2013).